Identification of Uromodulin Deposition in the Stroma of Perinephric Fibromyxoid Nephrogenic Adenoma by Mass Spectrometry

Kaori Yoshimura
Kanazawa University Hospital
Yukinobu Ito
yukinobuito@med.kanazawa-u.ac.jp
Kanazawa University
Mina Suzuki
Kanazawa University
Masafumi Horie
Kanazawa University
Takumi Nishiuchi
Kanazawa University
Yukako Shintani-Domoto
Nippon Medical School Hospital
Kazuyoshi Shigehara
Kanazawa University
Hiroko Ohshima
Kanazawa University
Masanobu Ohshima
Kanazawa University
Akiteru Goto
Akita University
Takayuki Nojima
Kanazawa University Hospital
Toyonori Tsuzuki
Aichi Medical University
Atsushi Mizokami
Kanazawa University
Hiroko Ikeda
Kanazawa University Hospital
Daichi Maeda

Kanazawa University

Case Report

Keywords: nephrogenic adenoma, fibromyxoid, uromodulin, Tamm-Horsfall protein, mass spectrometry

Posted Date: April 12th, 2023

DOI: https://doi.org/10.21203/rs.3.rs-2732966/v1

Additional Declarations: No competing interests reported.

Version of Record: A version of this preprint was published at Pathology International on January 30th, 2024. See the published version at https://doi.org/10.1111/pin.13409.

Abstract

Background

Nephrogenic adenoma (NA) is an epithelial lesion that usually occurs in the mucosa of the urinary tract. Rare cases of deep infiltrative or perinephric lesions have also been reported. Recently, NA with characteristic fibromyxoid stroma (fibromyxoid NA) has been proposed as a distinct variant. Although shedding of distal renal tubular cells due to urinary tract disorder has been postulated as the cause of NA in general, the mechanism underlying extraurinary presentation of NA and fibromyxoid stromal change in fibromyxoid NA remains unknown.

Case presentation:

An 82-year-old man had distal ureteral carcinoma and underwent total nephroureterectomy. The patient had no prior history of urinary tract injury or radiation. Periodic acid-Schiff staining-positive eosinophilic deposits were seen in the periureteral and perinephric regions proximal to the ureteral carcinoma. The eosinophilic structureless deposits in the stroma of fibromyxoid NA were microdissected and subjected to liquid chromatography/mass spectrometry (LC/MS). The analysis revealed the presence of a substantial amount of uromodulin (Tamm–Horsfall protein).The presence of urinary content in the stroma of perinephric fibromyxoid NA suggests that urinary tract failure and engraftment of renal tubular epithelial cells directly cause the lesion.

Conclusions

In conclusion, we reported a rare case of perinephric fibromyxoid NA with uromodulin deposits. In this study, proteomics analysis suggested the involvement of urinary material leakage. Mass spectrometry may be most effective when performed in lesions showing a characteristic morphology, especially in the stroma.

Background

Nephrogenic adenoma (NA) is a rare benign epithelial lesion that can occur in any part of the urinary tract, i.e., from the renal pelvis to the urethra [1]. NA occurs mostly in the bladder, followed by the urethra and ureter, but may also be seen in the renal pelvis and prostate [1]. The morphological features of NA include epithelial cells arranged in tubular, papillary, flat, microcystic, signet-ring cell-like, and vessel-like structures [2, 3]. Several clinical factors are involved in the development of NA, including genitourinary trauma, chronic inflammation, prior surgery, renal calculi, repeated instrumentation, anatomical anomalies, and pelvic radiation [4–6]. The epithelium is characterized by PAX8 immunopositivity in NA, suggesting a renal distal tubular origin [7, 8], and the disease is thought to be caused by the leakage of exfoliated epithelial cells from the prior injury site in the urinary tract.

Fibromyxoid NA is a rare variant characterized by epithelial cells surrounded by characteristic fibromyxoid stroma [9, 10]. A recent study by Li et al. showed that this variant of NA occurs predominantly in the bladder (80%), followed by the urethra (15%) and ureter (5%) [9]. The extent of fibromyxoid stromal change varies between cases, with 65% showing mixed classical and fibromyxoid NA morphology and the remaining 35% showing pure fibromyxoid morphology [9]. PAX8 immunoreactivity, which is an immunohistochemical hallmark of classical NA, was also observed in the epithelial cells of fibromyxoid NA [9]. The characteristic background matrix of fibromyxoid NA was reported to be strongly periodic acid-Schiff (PAS)-positive but negative for amyloid (Congo red) and reticulin staining [10]. There have been few studies of the substance comprising the background matrix of fibromyxoid NA, and mass spectrometry has not been applied to address this issue.

Although NA is usually limited to the lamina propria, rare cases showing infiltrative growth into the perinephric adipose tissue (perinephric NA) have also been reported. Focal fibromyxoid morphology was noted in one of the three cases of perinephric NA documented by Diolombi et al. [11]. In a series of fibromyxoid NAs, Li et al. also reported a case with involvement of perinephric fat [9]. Biopsy-associated perforation and extensive disruption due to hemorrhage or mechanical obstruction have been postulated as possible causes of these deep infiltrative NAs. However, the precise mechanism underlying the development of NA in extraurinary connective tissue remains unknown.

We recently encountered a rare case of perinephric fibromyxoid NA that extended to the periureteral region. To investigate the possible involvement of urinary leakage in its pathogenesis, we performed liquid chromatography/mass spectrometry (LC/MS) analysis of the stromal component of NA.

Case Presentation

Case

An 82-year-old man underwent full-body computed tomography (CT) for workup of an anterior mediastinal tumor, which unexpectedly revealed a right ureteral tumor, proximal ureteral dilatation, and right hydronephrosis. He had no prior history of urinary tract disease, radiotherapy, or Bacillus Calmette-Guérin (BCG) therapy. Retrograde ureterography revealed a defect area in the lower ureter, suggesting lower ureteral cancer. The urine cytology was positive for cancer cells. Biopsy was not performed prior to surgery. Retroperitoneoscopic right nephroureterectomy was performed.

Macroscopically, a grayish white polypoid mass measuring 23 × 10 × 10 mm obstructing the right distal ureter was observed. The proximal ureter and right renal pelvis were dilated. Irregularly distributed brownish areas were found in the renal hilar adipose tissue and periureteral tissue. A total of 37 sections were made from the kidney and ureteral tissues of the nephroureterectomy specimen. The ureter was sectioned *in toto.* We mapped the distribution of the fibromyxoid stroma with eosinophilic deposits based on morphological evaluation of hematoxylin and eosin (H&E)-stained sections, which mostly contained scattered epithelium (fibromyxoid NA) (Fig. 1).

Histological findings

Histologically, the ureteral tumor was classified as noninvasive low-grade urothelial carcinoma. Amorphous eosinophilic material deposits, stromal fibrosis, mild mononuclear cell infiltration, and hemorrhagic changes were observed in the background adipose tissue of the proximal periureteral and perinephric regions. Areas of eosinophilic deposition were mapped on the gross picture of the resected specimen (Fig. 1). The deposited areas were located proximal to the ureteral tumor and were not found distally. The deposited areas were multifocal, and their contours were irregular (Fig. 2A). The intensity of deposition varied between areas; some were dense and hyaline-like (Fig. 2B and 2C), whereas others were pale and pinkish. The hyaline-like deposits were positive on PAS staining (Fig. 2D), and negative on Congo red and phosphotungstic acid-hematoxylin staining. The pattern of elastic-Van Gieson staining was different from those of collagen and fibrin. Scattered nests and tubules of epithelial cells were identified in the background of the stromal fibroblasts (Fig. 2E and 2F). Some nests consisted of compressed cells with short-spindled nuclei. The tubular structures were generally small and atrophic. The epithelial cells had bland nuclei and mitoses were not found. The distribution of epithelial cells in the background of eosinophilic deposits was widespread, extending from the renal hilus to the periureteral adipose tissue.

Double staining with cytokeratin immunostaining and periodic acid-Schiff staining

To assess the relation between the intensity of eosinophilic deposits and distribution of epithelial cells, we performed double staining with cytokeratin immunostaining and PAS. Immunohistochemical staining was performed using a Ventana BenchMark XT system (Roche Diagnostics International AG) with anti-cytokeratin antibody (mouse monoclonal antibody, clone AE1/AE3; Dako Corp.) (dilution 1:1). Following cytokeratin staining, the slides were stained with PAS.

On cytokeratin-PAS double-stained slides, abundance of epithelium was not proportional with the amount of PAS-positive deposits. There were also areas of PAS-positive deposition without epithelium. Deposition was not always centered around the epithelium (Fig. 2G, 2H).

Immunohistochemical findings

A representative paraffin block containing fibromyxoid NA was cut into 4-μm-thick sections that were subjected to immunohistochemical staining using anti-cytokeratin 7 antibody (mouse monoclonal antibody, clone OV-TL 12/30; Dako Corp, Carpinteria, CA, USA) (dilution 1:75), anti-cytokeratin 20 antibody (mouse monoclonal antibody, clone Ks20.8; Dako Corp.) (dilution 1:75), anti-AMACR antibody (rabbit monoclonal antibody, clone 13H4; Dako Corp.) (dilution 1:100), anti-PAX8 antibody (mouse monoclonal antibody, clone MRQ-50; Roche Diagnostics International AG, Basel, Switzerland) (dilution 1:1), anti-GATA3 antibody (mouse monoclonal antibody, clone L50-823; Biocare Medical, LLC, Pacheco, CA, USA) (dilution 1:250), anti-ER antibody (rabbit monoclonal antibody, clone SP1; Roche Diagnostics International AG) (dilution 1:1), and anti-prostate-specific antigen (PSA) antibody (mouse monoclonal

antibody, clone ER-PR8; Dako Corp.) (dilution 1:75). Immunostaining was performed using a Ventana BenchMark ULTRA system (Roche Diagnostics International AG) according to the manufacturer's protocols. Appropriate controls were included.

Immunohistochemically, the epithelial cells were positive for CK7, AMACR, and PAX8 and negative for CK20, GATA-3, PSA, and estrogen receptor (ER) (Fig. 3). Based on the histopathological, histochemical, and immunohistochemical findings, a diagnosis of perinephric fibromyxoid NA was made.

Mass spectrometry of hyaline-like deposits around fibromyxoid nephrogenic adenoma

Formalin-fixed paraffin-embedded tissue of perinephric tissue containing fibromyxoid NA was cut into 10-μm-thick sections that were stained with H&E. Areas where PAS-positive eosinophilic deposits were present were microdissected using a laser microdissection device (Leica LMD7000; Leica Microsystems, Wetzlar, Germany). The background perinephric adipose tissue without deposits was also microdissected as a control. Microdissected tissue was collected into 0.5-ml microcentrifuge tubes containing 35 μl of a mixture of 10 mM Tris, 1 mM EDTA, and 0.002% Zwitterget. The protein was then eluted at 98°C for 90 min with occasional vortex mixing and sonicated for 60 min in a water bath. Mass spectrometry was performed as described previously [12].

To comprehensively explore deposits around fibromyxoid NA, we performed mass spectrometry on the microdissected PAS-positive eosinophilic deposits found in the stroma of fibromyxoid NA (Fig. 4A, 4B), in addition to the background adipose tissue (Fig. 4C, 4D). We identified 426 and 490 proteins with medium to high confidence according to the false discovery rate (FDR) in the eosinophilic deposits and background periureteral adipose tissue, respectively. After subtracting the background signal, 159 proteins were detected specifically in the deposited area (Fig. 4E) and uromodulin (UMOD) was the most abundant protein in the stroma of fibromyxoid NA (Table 1).

Table 1. Top 20 proteins identified exclusively in the eosinophilic deposits of fibromyxoid nephrogenic adenoma

Accession	Gene Symbol	Description	Sum PEP Score	Coverage [%]	Peptides	Biological Process	Cellular Component	Molecular Function
P07911	UMOD	Uromodulin	77.431	28	17	cell adhesion	non-structural extracellular	extracellular structural activity
B1ALD9	POSTN	Periostin	49.01	23	15	cell adhesion		
P00450	CP	Ceruloplasmin	46.563	17	13	transport	non-structural extracellular	other molecular function
C9JU00	FGG	Fibrinogen gamma chain	42.292	55	10	cell organization and biogenesis	non-structural extracellular	signal transduction activity
B7ZKJ8	ITIH4	ITIH4 protein	38.75	12	9		non-structural extracellular	enzyme regulator activity
P01031	C5	Complement C5	32.07	9	15	stress response	non-structural extracellular	signal transduction activity
Q99715	COL12A1	Collagen alpha-1(XII) chain	30.281	5	12	cell adhesion	extracellular matrix	extracellular structural activity
P02748	C9	Complement component C9	26.534	16	10	cell organization and biogenesis	non-structural extracellular	
P01859	IGHG2	Immunoglobulin heavy constant gamma 2	25.981	27	9	cell organization and biogenesis	non-structural extracellular	signal transduction activity
A0A4W9A917	IGHG3	Immunoglobulin heavy constant gamma 3	24.251	20	8			
P23142	FBLN1	Fibulin-1	21.589	10	7	cell organization and biogenesis	non-structural extracellular	signal transduction activity
Q15113	PCOLCE	Procollagen C-endopeptidase enhancer 1	20.66	24	6	protein metabolism		enzyme regulator activity
P04114	APOB	Apolipoprotein B-100	19.627	2	9	cell organization and biogenesis	non-structural extracellular	signal transduction activity
B4E1Z4		C3/C5 convertase	19.179	6	7	protein metabolism	non-structural extracellular	other molecular function
P29622	SERPINA4	Kallistatin	18.614	18	7			enzyme regulator activity
S4R460		Immunoglobulin heavy variable 3/OR16-9	18.465	31	2			
P36955	SERPINF1	Pigment epithelium-derived factor	18.103	20	6	cell cycle or cell proliferation	non-structural extracellular	enzyme regulator activity
P07358	C8B	Complement component C8 beta chain	18.058	11	6	stress response	non-structural extracellular	other molecular function
P11021	HSPA5	Endoplasmic reticulum chaperone BiP	17.206	11	6	protein metabolism	plasma membrane	translation activity
P04004	VTN	Vitronectin	17.187	9	5	cell adhesion	non-structural extracellular	signal transduction activity

Discussion And Conclusions

UMOD, also known as Tamm–Horsfall protein (THP), is a high molecular weight glycoprotein synthesized exclusively in the ascending loop of Henle by distal tubular cells in the normal kidney [8]. UMOD is the most abundant protein in urine. Mutation of the *UMOD* gene causes autosomal dominant tubulointerstitial kidney disease (ADTKD-UMOD), which is histologically characterized by abnormal accumulation of UMOD in renal tubular cells that can be identified by PAS staining [13]. In several pathogenic conditions, UMOD deposits are found in the renal parenchyma, perirenal soft tissue, renal hilar lymph node, or wall of the urinary bladder [8]. Histologically, UMOD deposition typically shows a “waxy” eosinophilic appearance. When the deposition amount is large, diagnosis is relatively straightforward even by H&E staining. In this study, we analyzed the substance deposited in the background stroma in a rare case of fibromyxoid NA involving perinephric and periureteral tissue. PAS-positive eosinophilic material, the morphology of which raised suspicion of UMOD deposition, was present. However, UMOD deposition had not been documented previously in fibromyxoid NA. In a series of eight cases of fibromyxoid NA, Hansel et al. performed immunohistochemistry for UMOD in three cases, all of which were negative [10]. In a series of 18 cases of urinary bladder UMOD deposition, Truong et al. reported the coexistence of NA in 2 cases [8]. However, apart from the areas of UMOD deposition, it is unclear whether these were cases of fibromyxoid NA or NA. As there were a number of candidates for the deposited substances, we applied a proteomics approach (LC/MS) to comprehensively investigate the proteins comprising the deposits. The results confirmed UMOD deposition in fibromyxoid NA.

Several factors have been implicated in the pathogenesis of NA, including genitourinary trauma, chronic inflammation, prior surgery, renal calculi, repeated instrumentation, irritation anatomical anomalies, and pelvic radiation [4, 6]. It is becoming increasingly common to view NA as a heterotopic autograft resulting

from renal tubular cells spilling into the urinary tract due to minor injury [11]. Based on the perirenal and periureteral stromal deposition of UMOD, along with the presence of epithelium of distal renal tubular lineage (i.e., positive for PAX8), we concluded that the extravasation of urinary contents is the key factor underlying the development of perinephric and/or fibromyxoid NA. In our case, eosinophilic deposits and scattered epithelium were observed on the proximal side of the ureteral carcinoma, but not in the distal ureter. Hydroureter and hydronephrosis were present. As no maneuvers that could cause mechanical damage to the urinary tract had been performed prior to the surgery, we assumed that increased luminal pressure due to obstruction by ureteral cancer led to urinary tract failure and leakage of urine into the surrounding stroma. Another possible mechanism of perinephric fibromyxoid NA formation is local production of UMOD by preexisting distal tubular epithelium in perinephric adipose tissue. In our case, however, there were areas with deposition only, i.e., without epithelium. Furthermore, the results of cytokeratin-PAS double staining demonstrated that deposition was not centralized around the epithelium. Therefore, we considered it unlikely that such processes (epithelium followed by UMOD deposition) had taken place.

Periostin (POSTN) was another protein detected exclusively in the deposition areas in this study. POSTN is an extracellular matrix protein abundantly expressed in collagen-rich connective tissue; its deposition is known to be induced by mechanical stress [14–16]. POSTN has also been reported to be present in neoplastic tissues, such as breast and colon cancers [17, 18]. Kikuchi et al. showed that POSTN is produced by cancer-associated fibroblasts in colon cancer [19]. In our case, stromal fibroblasts of fibromyxoid NA may have produced POSTN in response to infiltrating epithelium. Interestingly, other abundant proteins in the list, such as ceruloplasmin, fibrinogen, and ITIH4, are produced in the liver and secreted into the serum. Their presence in the stroma of fibromyxoid NA may have been due to leakage of serum contents, i.e., a result of hemorrhage. Further proteomics studies in larger NA case series are necessary to elucidate the complex architecture of the stroma and evaluate the frequency and distribution of UMOD deposition.

Perinephric fibromyxoid NA is a diagnostic challenge for surgical pathologists, especially if they are unaware of the lesion. Invasive adenocarcinoma is one of the differential diagnoses because the epithelium is scattered in the perinephric adipose tissue and often shows an infiltrative pattern. However, in fibromyxoid NA, the nuclei of the epithelium are completely bland, and mitoses are hardly seen. The absence of desmoplastic stromal reaction may be another finding excluding invasive cancer. A variety of benign lesions, such as remnant of Müllerian ducts, mesonephric duct derivatives, duplicate ureters, and ectopic prostatic glands, are also considered as differential diagnoses. The possibility of these lesions can be excluded by immunohistochemistry for lineage markers such as ER, GATA-3, PSA, and PAX8.

In conclusion, we reported a rare case of perinephric fibromyxoid NA. Proteomics analysis suggested the involvement of urinary leakage. Mass spectrometry is applied in limited contexts in the field of pathological diagnosis, mostly for classification of deposited amyloid [20–23]. This study indicated the potential of mass spectrometry for clarifying the pathogenesis of the disease. It is most effective when performed in lesions showing a characteristic morphology, especially in the stroma.

Abbreviations

FDR: false discovery rate

H&E: hematoxylin and eosin

LC/MS: liquid chromatography/mass spectrometry

NA: nephrogenic adenoma

PAS: periodic acid-Schiff

POSTN: periostin

THP: Tamm–Horsfall protein

UMOD: uromodulin

Declarations

Ethics approval and consent to participate.

All procedures were performed in accordance with the tenets of the Declaration of Helsinki. The study was approved by the institutional ethical committee of Kanazawa University (approval number: 12644-2).

Consent for publication

Informed consent for publication was obtained from the patient.

Availability of data and materials

The datasets generated during and/or analyzed during the current study are available from the corresponding author on reasonable request.

Competing interests

The authors declare no competing interests.

Funding

This study was funded by JSPS KAKENHI Grant Number JP 20K17948 to Yukinobu Ito, 22K06938 to Daichi Maeda.

Authors' contributions

Yukinobu Ito and Daichi Maeda conceptualized and designed the study. Kaori Yoshimura, Mina Suzuki, Kazuyoshi Shigehara and Atsushi Mizokami collected samples and provided clinical data. Takayuki Nojima, Toyonori Tsuzuki and Hiroko Ikeda provided histopathology expertise. Akiteru Goto and Daichi Maeda designed the experimental method. Yukako Shintani-Domoto, Hiroko Ohshima and Masanobu Ohshima supervised the experiment. Masafumi Horie and Takumi Nishiuchi performed acquisition of the data and the data analysis. Kaori Yoshimura and Yukinobu Ito wrote the first draft of the manuscript, and all authors critically revised the manuscript.

Kaori Yoshimura and Yukinobu Ito made equal contributions to the study.

Corresponding author:

Correspondence to Yukinobu Ito

Acknowledgements

This study was supported by JSPS KAKENHI Grant Number: JP 20K17948 to Yukinobu Ito, 22K06938 to Daichi Maeda.

References

1. Amin W, Parwani AV: **Nephrogenic adenoma**. *Pathology, research and practice* 2010, **206**(10):659-662.
2. Gordetsky J, Gennaro KH, Selph JP, Rais-Bahrami S: **Nephrogenic Adenoma: Clinical Features, Management, and Diagnostic Pitfalls**. *Urology* 2016, **95**:29-33.
3. Oliva E, Young RH: **Nephrogenic adenoma of the urinary tract: a review of the microscopic appearance of 80 cases with emphasis on unusual features**. *Modern pathology : an official journal of the United States and Canadian Academy of Pathology, Inc* 1995, **8**(7):722-730.
4. Chen C-S, Cheng C-L: **Nephrogenic Adenoma of the Urinary Bladder: Clinical Experience and Review of the Literature**. *Journal of the Chinese Medical Association* 2006, **69**(4):166-168.
5. de Buys Roessingh AS, Laurini RN, Meyrat BJ: **Nephrogenic adenoma of the urethra: an unusual cause of hematuria in the child**. *Journal of Pediatric Surgery* 2003, **38**(8):E8-E9.
6. Venyo AK: **Nephrogenic Adenoma of the Urinary Bladder: A Review of the Literature**. *International scholarly research notices* 2015, **2015**:704982.
7. Ozcan A, Shen SS, Hamilton C, Anjana K, Coffey D, Krishnan B, Truong LD: **PAX 8 expression in non-neoplastic tissues, primary tumors, and metastatic tumors: a comprehensive immunohistochemical study**. *Modern Pathology* 2011, **24**(6):751-764.
8. Truong LD, Ostrowski ML, Wheeler TM: **Tamm-Horsfall protein in bladder tissue. Morphologic spectrum and clinical significance**. *Am J Surg Pathol* 1994, **18**(6):615-622.

9. Li L, Williamson SR, Castillo RP, Delma KS, Gonzalgo ML, Epstein JI, Kryvenko ON: **Fibromyxoid Nephrogenic Adenoma: A Series of 43 Cases Reassessing Predisposing Conditions, Clinical Presentation, and Morphology**. *The American Journal of Surgical Pathology* 9900:10.1097/PAS.0000000000001986.
10. Hansel DE, Nadasdy T, Epstein JI: **Fibromyxoid Nephrogenic Adenoma: A Newly Recognized Variant Mimicking Mucinous Adenocarcinoma**. *The American Journal of Surgical Pathology* 2007, **31**(8).
11. Diolombi M, Ross HM, Mercalli F, Sharma R, Epstein JI: **Nephrogenic Adenoma: A Report of 3 Unusual Cases Infiltrating Into Perinephric Adipose Tissue**. *The American Journal of Surgical Pathology* 2013, **37**(4):532-538.
12. Sidiq Y, Tamaoki D, Nishiuchi T: **Proteomic Profiling of Plant and Pathogen Interaction on the Leaf Epidermis**. *International Journal of Molecular Sciences* 2022, **23**(20):12171.
13. Onoe T, Hara S, Yamada K, Zoshima T, Mizushima I, Ito K, Mori T, Daimon S, Muramoto H, Shimizu M *et al*: **Significance of kidney biopsy in autosomal dominant tubulointerstitial kidney disease-UMOD: is kidney biopsy truly nonspecific?** *BMC Nephrology* 2021, **22**(1):1.
14. Horiuchi K, Amizuka N, Takeshita S, Takamatsu H, Katsuura M, Ozawa H, Toyama Y, Bonewald LF, Kudo A: **Identification and characterization of a novel protein, periostin, with restricted expression to periosteum and periodontal ligament and increased expression by transforming growth factor beta**. *Journal of bone and mineral research : the official journal of the American Society for Bone and Mineral Research* 1999, **14**(7):1239-1249.
15. Norris RA, Damon B, Mironov V, Kasyanov V, Ramamurthi A, Moreno-Rodriguez R, Trusk T, Potts JD, Goodwin RL, Davis J *et al*: **Periostin regulates collagen fibrillogenesis and the biomechanical properties of connective tissues**. *Journal of cellular biochemistry* 2007, **101**(3):695-711.
16. Kruzynska-Frejtag A, Machnicki M, Rogers R, Markwald RR, Conway SJ: **Periostin (an osteoblast-specific factor) is expressed within the embryonic mouse heart during valve formation**. *Mechanisms of development* 2001, **103**(1-2):183-188.
17. Sasaki H, Yu CY, Dai M, Tam C, Loda M, Auclair D, Chen LB, Elias A: **Elevated serum periostin levels in patients with bone metastases from breast but not lung cancer**. *Breast cancer research and treatment* 2003, **77**(3):245-252.
18. Bao S, Ouyang G, Bai X, Huang Z, Ma C, Liu M, Shao R, Anderson RM, Rich JN, Wang X-F: **Periostin potently promotes metastatic growth of colon cancer by augmenting cell survival via the Akt/PKB pathway**. *Cancer Cell* 2004, **5**(4):329-339.
19. Kikuchi Y, Kashima TG, Nishiyama T, Shimazu K, Morishita Y, Shimazaki M, Kii I, Horie H, Nagai H, Kudo A *et al*: **Periostin is expressed in pericryptal fibroblasts and cancer-associated fibroblasts in the colon**. *The journal of histochemistry and cytochemistry : official journal of the Histochemistry Society* 2008, **56**(8):753-764.
20. Larsen BT, Mereuta OM, Dasari S, Fayyaz AU, Theis JD, Vrana JA, Grogan M, Dogan A, Dispenzieri A, Edwards WD *et al*: **Correlation of histomorphological pattern of cardiac amyloid deposition with**

amyloid type: a histological and proteomic analysis of 108 cases. *Histopathology* 2016, **68**(5):648-656.

21. Dasari S, Theis JD, Vrana JA, Meureta OM, Quint PS, Muppa P, Zenka RM, Tschumper RC, Jelinek DF, Davila JI *et al*: **Proteomic detection of immunoglobulin light chain variable region peptides from amyloidosis patient biopsies**. *Journal of proteome research* 2015, **14**(4):1957-1967.
22. Chapman JR, Liu A, Yi SS, Hernandez E, Ritorto MS, Jungbluth AA, Pulitzer M, Dogan A: **Proteomic analysis shows that the main constituent of subepidermal localised cutaneous amyloidosis is not galectin-7**. *Amyloid : the international journal of experimental and clinical investigation : the official journal of the International Society of Amyloidosis* 2021, **28**(1):35-41.
23. Shintani-Domoto Y, Ishino K, Naiki H, Sakatani T, Ohashi R: **Autopsy case with concurrent transthyretin and immunoglobulin amyloidosis**. *Pathology International* 2022, **72**(1):65-71.

Figures

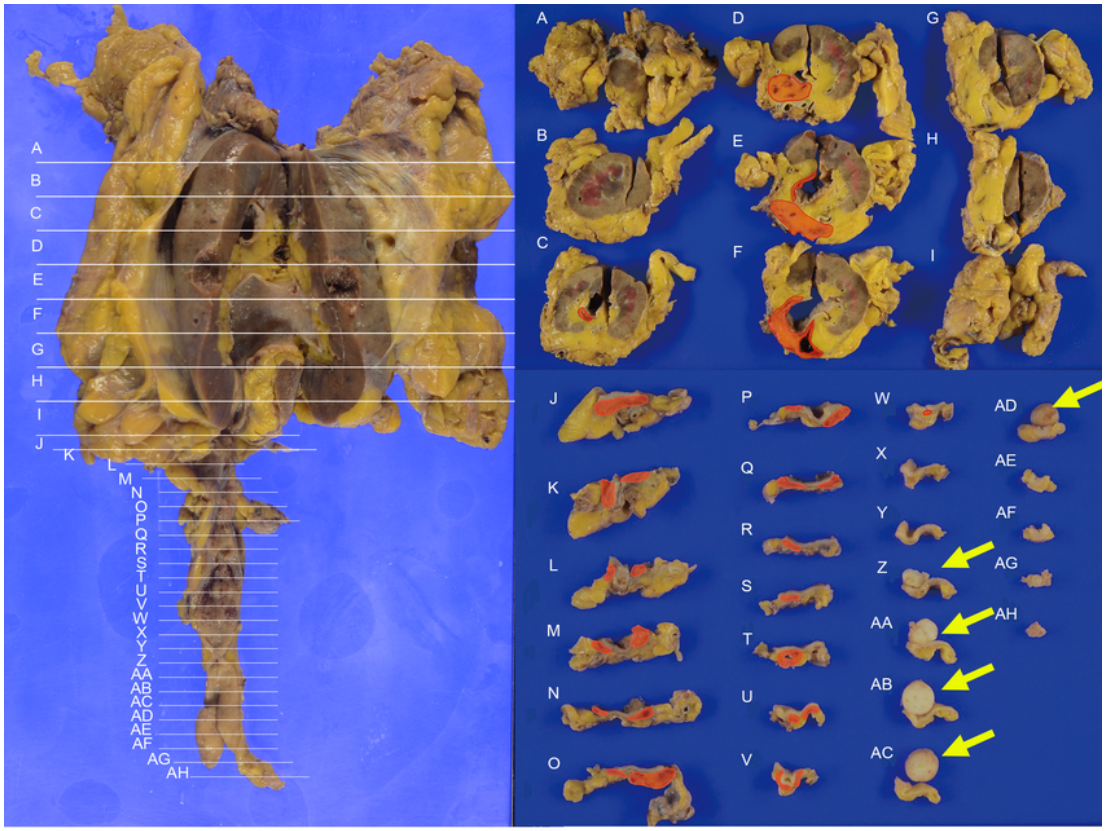

Figure 1

Gross picture of nephroureterectomy specimen and its cut surfaces

A polypoid urothelial carcinoma was present in the distal ureter (yellow arrows). The proximal ureter and renal pelvis were dilated (hydronephrosis and hydroureter). The areas of stromal deposition of eosinophilic material are shown in red; they were located mainly in the adipose tissue of the renal hilum,

and in perinephric and periureteral regions. In most of the deposition areas, scattered epithelium was present. The lesion represented fibromyxoid nephrogenic adenoma.

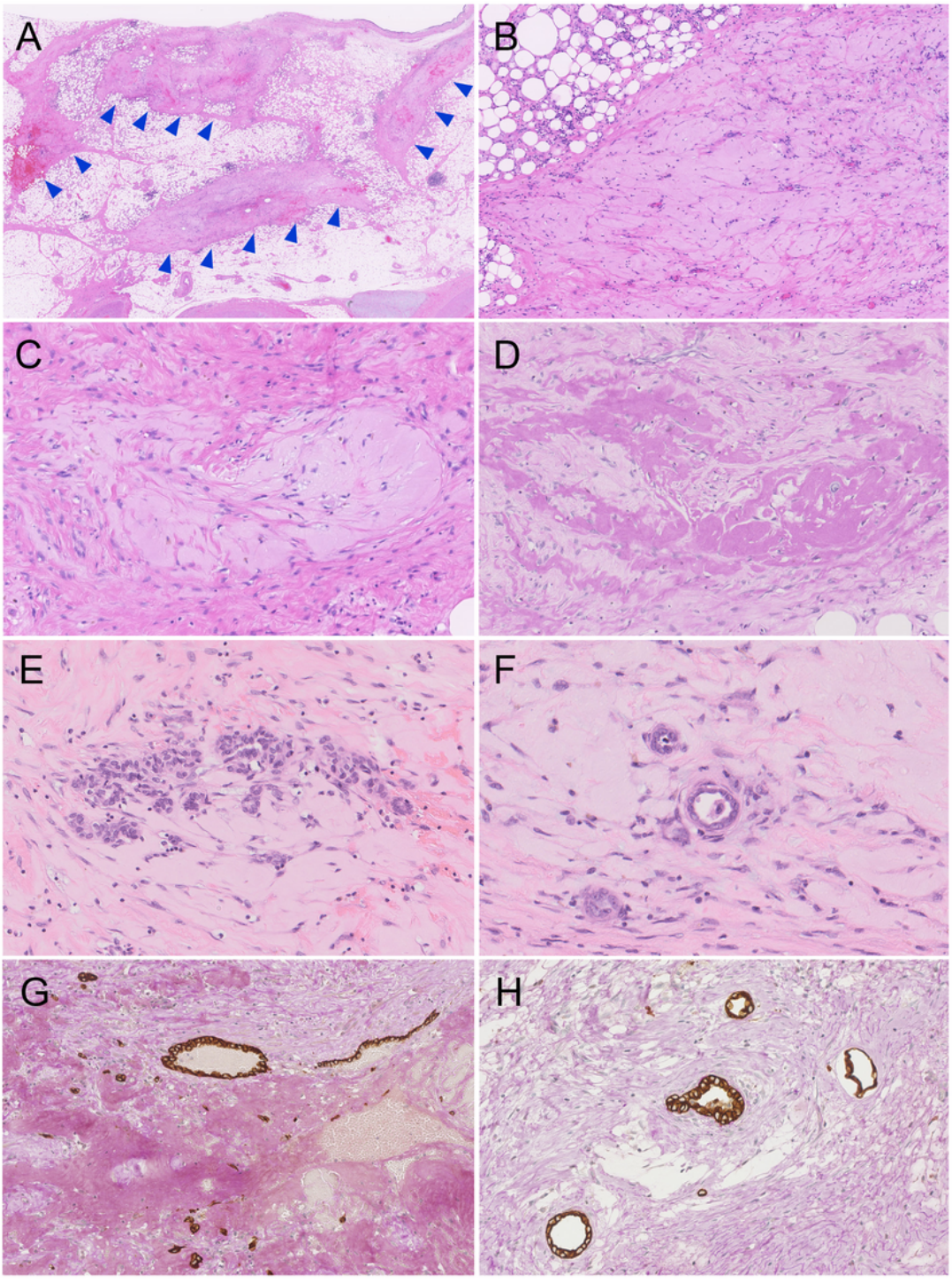

Figure 2

Microscopic findings of perinephric fibromyxoid nephrogenic adenoma

A: Low-power view of perinephric adipose tissue with irregularly distributed areas of eosinophilic deposition and stromal fibrosis (arrowheads). Focal hemorrhagic changes were seen.

B: Area with eosinophilic deposition. Intervening fibrous tissue and vascular structures were present. Mild mononuclear cell infiltration was observed in the surrounding stroma.

C: High-power view of amorphous and hyaline-like eosinophilic deposition.

D: Strong PAS positivity of the deposited material.

E. Epithelial component interspersed in the background of eosinophilic deposition. The epithelial cells were bland, with round to ovoid nuclei, and formed small nests and glands.

F: Glandular structure of fibromyxoid nephrogenic adenoma (NA). A monolayer of epithelial cells lined the lumen.

G: Cytokeratin-PAS double staining of NA. Cytokeratin-positive epithelium was identified in the background of PAS-positive stroma. The intensity of PAS positivity varied between areas and deposition was not centered around the epithelium.

H. Cytokeratin-PAS double staining of NA. Epithelium was also present in the area without eosinophilic deposition.

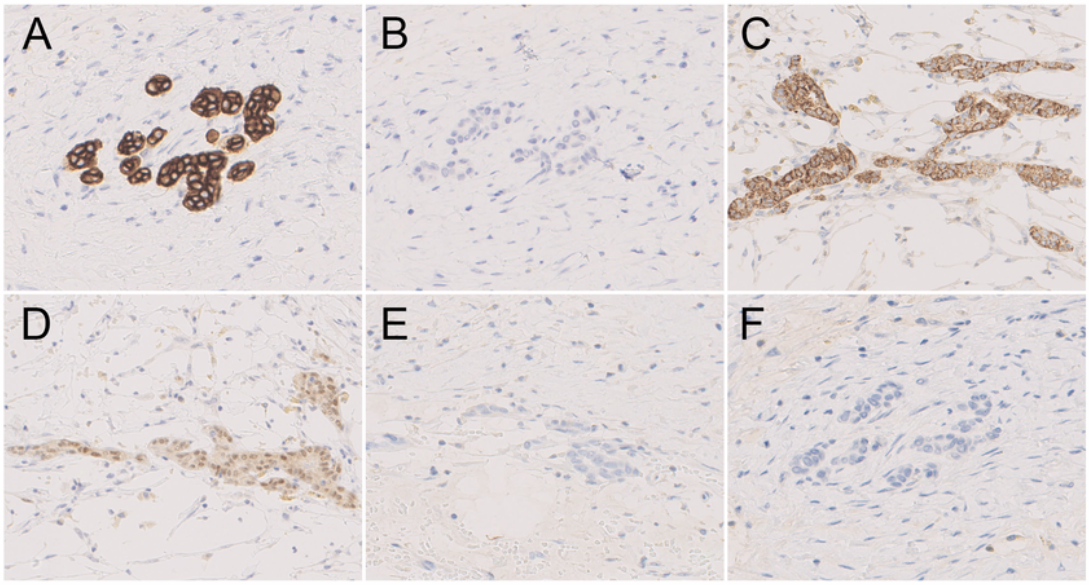

Figure 3

Immunohistochemical features of the epithelial cells of perinephric fibromyxoid nephrogenic adenoma

Immunohistochemically, the tumor cells were positive for (A) CK7, (B) AMACR, and (C) PAX8, and negative for (D) CK20, (E) GATA-3, and (F) PSA.

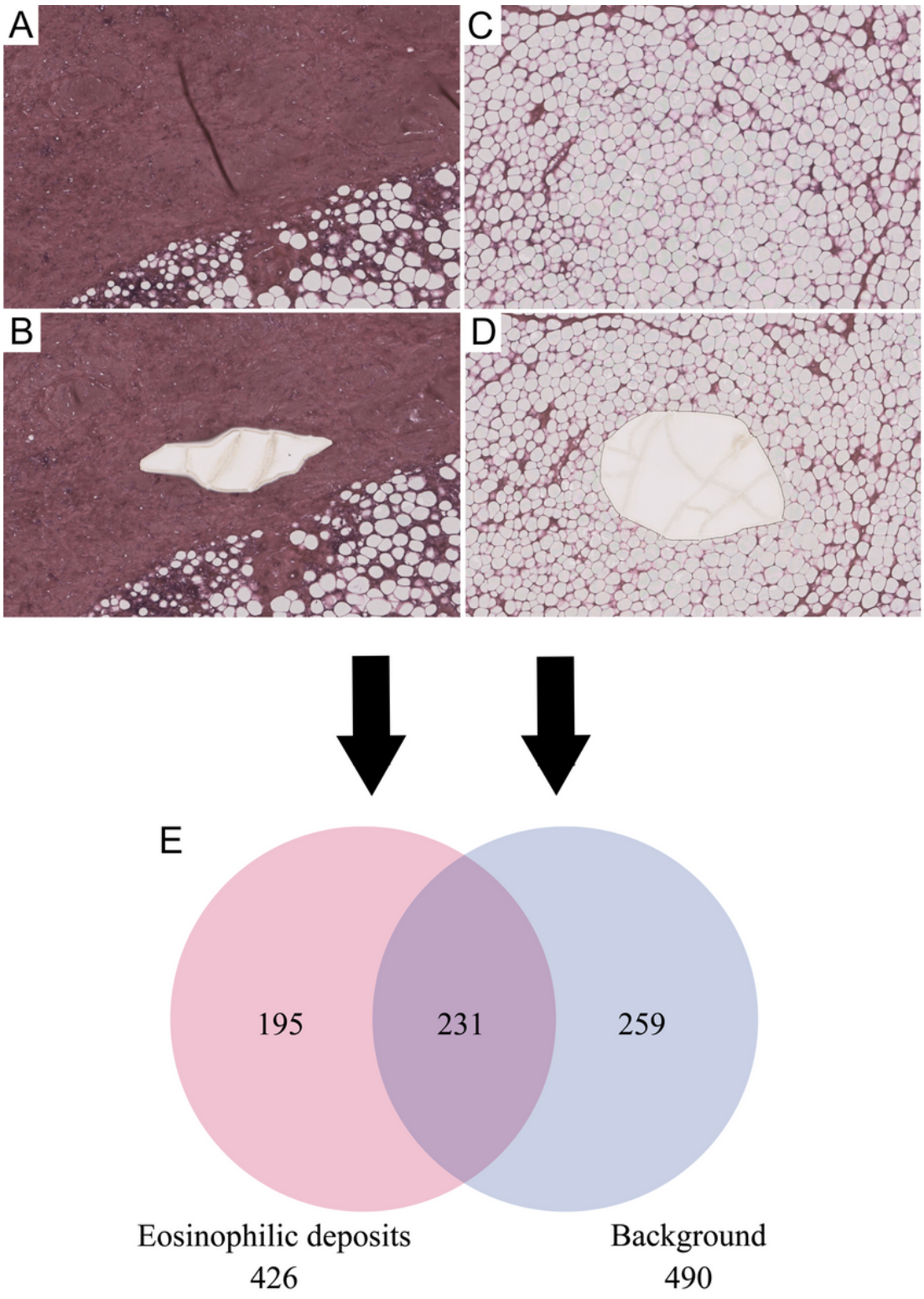

Figure 4

Proteomic comparison of eosinophilic deposits and background adipose tissue

The area of perinephric eosinophilic deposits without epithelium (A) prior to microdissection and (C) after microdissection. The area of background adipose tissue without deposition (B) prior to microdissection and (D) after microdissection. (E) Venn diagram showing the number of proteins identified in eosinophilic

deposits with background adipose tissue. A total of 426 significant proteins were identified in the eosinophilic deposits and 490 were identified in the background. We detected 195 proteins exclusively in the deposited material, which included uromodulin.